HAL
archives-ouvertes.fr

The truncated prelamin A in Hutchinson-Gilford progeria syndrome alters segregation of A-type and B-type lamin homopolymers.

Erwan Delbarre, Marc Tramier, Maïté Coppey-Moisan, Claire Gaillard,

Jean-Claude Courvalin, Brigitte Buendia

HAL Id: hal-00019639

https://hal.archives-ouvertes.fr/hal-00019639

Submitted on 24 Feb 2007

The truncated prelamin A in Hutchinson-Gilford progeria syndrome alters segregation of A-type and B-type lamin homopolymers

Erwan Delbarre, Marc Tramier, Maïté Coppey-Moisan, Claire Gaillard, Jean-Claude Courvalin and Brigitte Buendia

Département de Biologie Cellulaire, Institut Jacques Monod, UMR 7592 CNRS
Université Paris 6 & 7, 2 Place Jussieu, 75251 Paris Cedex 05, France

Corresponding author :
Dr Brigitte Buendia
Institut Jacques Monod
Tour 43, 2, place Jussieu
75251 Paris Cedex 05 France
TEL : + 33 1 44 27 77 65
FAX : + 33 1 44 27 59 94

ABSTRACT

Hutchinson-Gilford progeria syndrome (HGPS) is a dominant autosomal premature aging syndrome caused by the expression of a truncated prelamin A designated progerin. A-type and B-type lamins are intermediate filament proteins that polymerize to form the nuclear lamina network apposed to the inner nuclear membrane of vertebrate somatic cells. It is not known if *in vivo* both type of lamins assemble independently or coassemble. The blebbing and disorganization of the nuclear envelope and adjacent heterochromatin in cells from patients with HGPS is a hallmark of the disease, and the *ex vivo* reversal of this phenotype is considered important for the development of therapeutic strategies. Here we investigated the alterations in the lamina structure that may underlie the disorganization caused in nuclei by progerin expression. We studied the polymerization of EGFP- and DsRed-tagged wild-type and mutated lamins in the nuclear envelope of living cells by measuring fluorescence resonance energy transfer (FRET) that occurs between the two fluorophores when tagged lamins interact. Using time domain fluorescence lifetime imaging microscopy (tdFLIM) that allows a quantitative analysis of FRET signals, we show that wild-type lamins A and B1 polymerize in distinct homopolymers that further interact in the lamina. In contrast, expressed progerin coassembles with lamin B1 and lamin A to form a mixed heteropolymer in which A-type and B-type lamin segregation is lost. We propose that such structural lamina alterations may be part of the primary mechanisms leading to HGPS, possibly by impairing functions specific for each lamin type such as nuclear membrane biogenesis, signal transduction, nuclear compartmentalization and gene regulation.

INTRODUCTION

Lamins are nuclear intermediate filament proteins with a central dimerization domain or rod (Fig. 1A) that polymerize to form the lamina network underlying the inner nuclear membrane (1). Lamina forms a highly stable structure (2) and anchors nuclear pore complexes, heterochromatin and regulatory proteins at the nuclear periphery (3). B-type lamins are constitutive whereas A-type lamins (lamins A and C) which arise from the LMNA gene by alternative splicing (1, 4) are expressed only in differentiated cells (5). Lamin A is synthesized as a precursor, prelamin A, that terminates with a CAAX motif (4). This motif triggers sequential posttranslational modifications: farnesylation of the cysteine, removal of the AAX amino acids by the endoprotease Zmpste24, and carboxymethylation of the cysteine (6-8). After completion of these modifications, the last 15 amino acids of prelamin A, including the modified cysteine, are also cleaved by the Zmpste24 endoprotease, generating mature lamin A (6-10). The interactions of A- and B-type lamins have been investigated by biochemical methods (11-14) and two-hybrid analyses (15) and homotypic and heterotypic interactions were detected. Whether *in vivo* lamins coassemble or assemble independently at the membrane-chromatin interface of somatic cell nuclei is unknown.

Mutations in the LMNA gene cause a wide array of inherited diseases, including myopathies, a partial lipodystrophy, a peripheral neuropathy, and premature aging syndromes (16). Hutchinson-Gilford progeria syndrome (HGPS) is a dominant autosomal premature aging disease due to the expression of a truncated prelamin A designated progerin. HGPS is most commonly caused by a point mutation in exon 11 of LMNA that activates a cryptic donor splice site (17, 18). This mutation leads to the deletion of 50 amino acids within prelamin A that leaves the CAAX motif intact but removes the final endoproteolytic cleavage site. Hence, the mutant prelamin A is predicted to undergo post-translational modification of the terminal cysteine that will be retained in progerin (19-23). Expression of progerin in cells of subjects with HGPS triggers an increase in perimeter length of nuclei with an extensive folding of the nuclear envelope, accompanied by a modification of the ultrastructural organization of the lamina and chromatin (24). Misshapen nuclei in HGPS have been considered as the cellular disease phenotype, whose recovery is used as a test for therapeutic efficiency. This nuclear phenotype is reversed upon splicing correction of prelamin A pre-mRNA (25), or by blocking the farnesyltransferase (19-23)

Here we analyzed the alterations in the lamina structure that may underlie the disorganization caused in the nuclear envelope by progerin expression. We studied the interactions between EGFP- and DsRed-tagged wild-type and mutated lamins in the nuclear envelope of living cells by measuring fluorescence resonance energy transfer (FRET), using a quantitative method, time domain fluorescence lifetime imaging microscopy (tdFLIM). We first studied the interactions of wild-type A- and B-type lamins, in an attempt to establish a putative model of their assembly in the lamina. We then used the same approach to analyze how tagged-progerin integrates and/or disturbs the lamina network.

RESULTS

tdFLIM is an appropriate method to study lamin-lamin interactions in living cells

We used tdFLIM to detect energy transfer between lamins tagged with EGFP and DsRed fluorescent molecules because this method possesses features that are most appropriate for the study of protein-protein interactions within polymers. Briefly, when an EGFP-tagged protein (donor) interacts with a DsRed-tagged protein (acceptor) in a cotransfected cell, FRET can occur if the distance between the two fluorophores is less than 10 nm, leading to a faster fluorescence decay of EGFP molecules. The fluorescence lifetime of EGFP molecules involved in FRET (τ_{FRET}) is shorter than that associated with the EGFP molecules that do not interact with DsRed (τ_{EGFP}). These two lifetimes allow the calculation of real FRET efficiency (E) through a simple equation ($E = 1 - \tau_{FRET}/\tau_{EGFP}$; see *Materials and Methods*). The measurement of this E value is the basis of the tdFLIM method since differences in E values will only reflect variations in the distance/orientation between the fluorescent molecules, but neither the variations in the cellular concentration of tagged molecules nor the variations in the relative concentrations of green and red species. This property of tdFLIM was essential for the present study because the dilution of the exogenous fluorescent lamins by endogenous lamins may vary from cell to cell, as well as the relative content in green and red fluorescent lamins. In most of the experiments presented here, lamins are tagged at their amino-terminal end (Fig. 1A). Once lamins tagged at this site are incorporated in the lamina, the orientation of their fluorophores is expected to be the same. We therefore interpret the differences in E values found for various lamin combinations as mostly reflecting differences in the distances separating the tagged lamins in the lamina (see *Materials and Methods)*. The second basic feature of tdFLIM is that it makes it possible to measure the proportion of EGFP-tagged molecules involved in FRET in a given cell. This proportion varies depending on two parameters, (i) the ratio of exogenous versus endogenous lamins (unknown at the level of individual cells), and (ii) the ratio of acceptor (Ds<u>R</u>ed) versus donor (E<u>G</u>FP) molecules, that is measured through the R/G ratio (see *Materials and Methods*). In a fraction of cells with an unfavorable balance between these two parameters, the probability of a close proximity of green and red fluorescent markers is low and FRET is undetectable. The measurement at a low R/G value of the fraction of cells with detectable FRET signals allowed us to compare the ability of diffent lamins to interact with each other (see below).

Overexpressed lamins are integrated within the lamina

Lamins tagged at their amino-terminal end (Fig. 1*A*) were transiently expressed in C2C12 myoblasts. A major characteristic of the nuclear lamina is its resistance to extraction by non ionic detergents and salt. We analyzed the resistance to extraction of exogenous and endogenous lamins in control C2C12 cells (Fig. 1B, upper panel), and in C2C12 cells overexpressing either DsRed-lamin A and EGFP-lamin B1 (Fig. 1B, middle panel) or EGFP-progerin (Fig. 1B, lower panel). Cells were sequentially extracted with Triton X-100, Triton and salt, and finally digested with DNase I and RNase A followed by salt extraction. Supernatants and the final insoluble fraction were analyzed by immunoblotting, using antibodies directed against lamins A and C, lamin B1, and EGFP. Exogenous lamins were as resistant to extraction as endogenous lamins (Fig. 1B), showing that they were integrated within the lamina.

The localization of the exogenous lamins at the nuclear envelope was confirmed by fluorescent microscopy data. In C2C12 cells that contain A- and B-type lamins and in P19 embryonic cells with only B-type lamins (26), exogenous wild-type and mutated lamins were targeted to the nuclear envelope with a pattern indistinguishable from that of endogenous lamins (Fig 2). Overexpression of lamin B1 induced in some cells an enlargment of the nucleus with nuclear envelope folding (Fig. 2A, arrowheads). A similar increase in size of the nucleus with occasional formation of herniations and blebs was observed in some cells overexpressing progerin (Fig. 2A, arrows).

Homotypic and heterotypic lamin interactions are detected within the lamina

We first investigated the occurrence of heterotypic interactions at the nuclear envelope of C2C12 cells transfected with plasmids encoding EGFP-lamin A and DsRed-lamin B1. Fig. 3*A* shows that the fluorescence decay of EGFP-lamin A at the nuclear envelope was more rapid in cotransfected cells (blue curve) than in monotransfected cells (green curve), signaling FRET occurrence. In monotransfected cells, the EGFP fluorescence decay was monoexponential with a lifetime (τ_{EGFP}) of 2.27 ± 0.07 ns (Table 1). In cells coexpressing tagged lamins in which FRET was detectable, fluorescence decay became faster due to the appearance of a shorter lifetime. As discussed above, this shorter lifetime (τ_{FRET}) corresponds to EGFP-lamin A molecules that interact with DsRed-lamin B1 (see also *Materials and Methods*). Whatever the lamin combination, DsRed-Lamin

B1/EGFP-lamin A or DsRed-La A/EGFP-lamin B1, similar values for τ_{FRET} and real FRET efficiency (E) were obtained ($\tau_{FRET} = 0.76 \pm 0.09$ ns and E = 0.66 ± 0.04 *versus* $\tau_{FRET} = 0.80 \pm 0.09$ ns and E = 0.65 ± 0.04, respectively) (Table 1). As negative control, we analyzed the interactions of lamins with Pom 121, a transmembrane nucleoporin that cannot interact with lamins for topological reasons (27). No FRET was detected when EGFP-Pom 121 was coexpressed with either DsRed-lamin B1 (Fig. 3B) or DsRed-lamin A (data not shown), whatever the levels of expression of lamins and Pom 121. These data that assess the existence of heterotypic interactions in the lamina of living cells are in agrement with the data of Moir et al. (28) who made similar observations in post-mitotic cells using a qualitative FRET method.

In cells coexpressing homologous lamins, FRET was also detected (Fig. 3C, Table 1), but the EGFP fluorescence lifetime and the corresponding real FRET efficiency of lamin B1 homotypic interactions ($\tau_{FRET} = 1.00 \pm 0.08$ ns; E = 0.57 ± 0.04) were distinct from those of lamin A homotypic interactions ($\tau_{FRET} = 0.83 \pm 0.09$ ns; E = 0.64 ± 0.04) (P < 0.0001) and from those of heterotypic interactions (see above; Table 1) (P < 0.0001). This difference means that the range of distances between lamin B1 molecules in lamina is different from that between lamin A molecules or between lamin A and lamin B1 molecules.

Interactions between exogenous lamins A and B1 were also tested in P19 cells that express B-type lamins but not A-type lamins (26). Heterotypic interactions were detected with a mean real FRET efficiency value (E = 0.65 ± 0.05) close to the value obtained in C2C12 cells (E = 0.65 ± 0.04) (Table 1). The similar FRET efficiency in two cell lines, one of which is devoid of endogenous A-type lamins, supports the scaffolding role postulated for B-type lamins in the assembly of lamin A (29). It is worth noting that the real FRET efficiency for homotypic lamin B1 interactions (E = 0.65 ± 0.05) was higher in P19 cells than in C2C12 cells (E = 0.57 ± 0.04; P < 0.0001) (Table 1), indicating that the range of distances between lamin B1 molecules in the lamina is different in the two cell lines. This suggests that the structure of lamin B1 polymers varies with the composition of the nuclear envelope, and in particular with the level of expressed lamin A. The conclusion from this series of experiments is that FRET occurred between homologous and heterologous tagged lamins in the lamina of living cells.

Lamin-lamin interactions detected by FRET occur within high order polymers

Since the first step in lamin polymerization is homodimerization (1, 30), heterotypic lamin A-lamin B1 interactions detected by FRET were only occurring between homodimers of both types in high order polymers. However, a plausible explanation for the homotypic interactions would be their occurrence at the very first stage of lamin assembly, within the homodimers. To check this possibility, we coexpressed homologous lamins tagged with the two fluorophores and analyzed mitotic cells in which the lamina is disassembled into distinct populations of A-type and B-type homodimers (30). No FRET was detected indicating that energy transfer did not occur within homodimers (data not shown). This suggests that in interphasic cells, FRET occurs between dimers within higher order polymers. To strengthen this hypothesis, we analyzed the signals generated in the nuclear envelope of interphasic C2C12 cells by coexpression of lamin A molecules tagged with EGFP or DsRed at different sites. One lamin A molecule was fused at its amino-terminal end to DsRed and another one with EGFP immediately after the rod domain (Fig. 1A, Intra-EGFP-La A). In a putative homodimer containing both fluorophores, FRET should not occur because the two tags would be separated by a distance roughly the length of the rod domain (~ 50 nm; see Fig. 1A), i.e. greater than the maximum distance compatible with FRET (10 nm). The data showed that FRET was detected between Intra-EGFP-lamin A and DsRed-lamin A with an associated lifetime of 0.94 ± 0.14 ns (n = 25). Real FRET efficiency (E = 0.59 ± 0.06) was lower than obtained when both tags were present at the amino-terminal end of lamin A (E = 0.64 ± 0.04; P < 0.001). This difference in E values is probably due to different distances between the fluorophores in the lamina and to possible distinct orientations related to their locations in lamin A. These data demonstrate that FRET signals did not occur between two lamin molecules within homodimers, but rather between lamins present in distinct dimers within higher order polymers.

Homotypic interactions are favored over heterotypic interactions

In cotransfected cells, it was checked if among the different lamin combinations used here some were more favorable than others in triggering FRET. The acceptor (DsRed) to donor (EGFP) ratio (R/G) was measured in individual cells and found to vary between 2 and 25 (Table 2; see *Materials and Methods*). In cells containing a large excess of acceptor over donor (R/G > 15), FRET was detected in all cells, whatever the lamin combination (Table 2). With a lower excess of acceptor over donor (R/G < 15), homotypic combinations generated a higher proportion of

cells positive for FRET than heterotypic combinations (Table 2, 83% and 93% versus 20%), meaning that the threshold for FRET triggering was lower for homotypic interactions. In the lamina, homotypic interactions are therefore clearly favored compared to heterotypic interactions.

Integration of progerin within the lamina

We then assessed how truncated prelamin A (progerin) integrates into the lamina. Figures 1B and 2A show that both EGFP- and DsRed-tagged progerin molecules are targeted to the nuclear envelope in C2C12 cells and incorporated into an extraction-resistant structure. As the toxic effect of progerin in cells is dose-dependent (24), FRET analyses were performed at a high level of progerin expression with progerin as the acceptor molecule (DsRed-progerin). When the tagged progerins were coexpressed, or when DsRed-progerin was expressed with EGFP-tagged lamins B1 or A, FRET occurred in all cases, with nearly identical real FRET efficiencies of 0.58 ± 0.07, 0.56 ± 0.07, and 0.59 ± 0.05, respectively (Table 1). Thus, the range of distances in the lamina separating progerin molecules from each other, from lamin A, and from lamin B1 is identical, supporting an even distribution of these three lamin proteins in the lamina. These similar real FRET efficiency values found for progerin interactions were lower than those previously found for lamin A interactions with either lamin A (E = 0.64 ± 0.04; P < 0.002) or lamin B1 (E = 0.65 ± 0.04; P < 0.0004) (Table 1). In contrast, the E values found for progerin interactions were similar to those previously measured for lamin B1 homotypic interactions (E = 0.57 ± 0.04), indicating that the common range of distances separating lamins A, B1, and progerin in the lamina is similar to that previously found between lamin B1 molecules. These data suggest that progerin behaves similarly as lamin B1 during lamina assembly. The fact that lamin B1 coassembles preferentially with progerin rather than with wild-type lamin A is supported by the high proportion of cells in which FRET was detectable when DsRed-progerin and EGFP-lamin B1 were coexpressed, compared to the low proportion when DsRed-lamin A and EGFP-lamin B1 were coexpressed (62% versus 20%; P < 0.05) (Table 2; R/G < 15). Taken together, our data support a model in which progerin would displace a pool of lamin A from homopolymers to a heterotypic structure containing also lamin B1 and progerin.

DISCUSSION

We used tdFLIM, a quantitative FRET analysis method, to study alterations in lamin polymerization in living cells provoked by the expression of progerin. Since the *in vivo* homo- or heteropolymerization of A- and B-type lamins had not been elucidated, the interactions of wild-type lamins of both types tagged with EGFP and DsRed were first studied, in an attempt to establish a putative model of their assembly in the lamina. Three possible models of lamin polymer organization were considered (Fig. 4A). In model 1, A-type and B-type lamins form homopolymers that are not in contact. In model 2, A-type and B-type lamins interact within heteropolymers where they are evenly distributed. In model 3, A-type and B-type lamins interact within polymers where they are not evenly distributed. We then checked with which model the FRET data fit the best. Since, as shown here, lamin A and lamin B1 interact, model 1 was discarded. An even distribution of lamins of both types into polymers, as in model 2, would have provided homogeneous real FRET efficiencies values and similar proportions of FRET positive cells at all R/G ratios, whatever the lamin combination. Instead, we obtained different values of real FRET efficiencies for the homotypic interactions of lamin A and lamin B1, and a low sensitivity for FRET triggered by heterologous combinations of lamins compared to both homologous combinations of lamins. These data eliminate model 2 and support model 3 that postulates an uneven distribution of lamins in polymers. Model 3 is compatible with either an heteropolymeric structure with an uneven distribution of both lamins or the juxtaposition of homopolymers of lamin A and lamin B1 in close contact. FRET analysis did not allow us to distinguish between these two possibilities, but the existence of homotypic structures of both lamin types in living cells supports the latter possibilities. In the nuclei of embryonic and stem cells, the lamina is exclusively composed of B-type lamins (5). On the contrary, nuclei in cultured fibroblasts of individuals expressing lamin A bearing missense mutations (31, 32) develop membrane herniations that contain a lamina structure exclusively composed of A-type lamins. Since homopolymerization of A- and B-type lamins were shown by these previous studies to occur in living cells and heterotypic interactions of lamins are demonstrated in the present study, we favor the model of lamina in which interaction occurs between juxtaposed A-type and B-type lamin homopolymers.

We further propose an additional feature of the lamina structure linked to the difference in post-translational modifications present at the carboxyl-terminal end of mature lamin B1 and

10

lamin A. B-type lamins are permanently farnesylated at their carboxyl-terminal end (7, 8), while this modification occurs only transiently in the process of prelamin A maturation, due to the action of the specific membranous endoprotease Zmpste24 (6, 8-10). We suggest that polymers of farnesylated B-type lamins associate more closely with the membrane than polymers of A-type lamins (Fig. 4B), due to the integration of the hydrophobic farnesyl group within the inner nuclear membrane and/or association with a putative isoprenyl-carboxymethyl-lamin receptor (33).

The same approach was used to analyze how tagged-progerin integrates and/or disrupts the lamina network. We showed that progerin can interact with both lamin A and lamin B1, as well as with progerin. The observation that real FRET efficiencies are the same for these lamin combinations (Table 1) supports an even distribution of the three lamin proteins in the lamina. The shared real FRET efficiency value was lower than that previously found for wild-type lamin A homotypic and heterotypic interactions, but similar to that measured for lamin B1 homotypic interactions. Thus, the range of distances separating progerin and lamins A and B1 in the lamina is identical to the range of distances separating lamin B1 molecules in homotypic polymers. These data suggest that progerin behaves as lamin B1 during lamina assembly. This conclusion was strengthened by the fact that lamin B1 preferentially coassembles with progerin rather than with wild-type lamin A (Table 2). Taken together, our data support a model in which progerin would displace a pool of lamin A from homopolymers to form a heterotypic structure containing evenly distributed lamin B1, progerin and lamin A (Fig. 4C). Expression of progerin would thus switch lamina structure from model 3 to model 2 (Fig. 4A).

This change in lamina assembly may explain how endogenous as well as exogenous progerin generate dysmorphic nuclei with extensive nuclear membranes (24, 25) (Fig. 2A). In normal cells, the cysteine residue post-translationally modified at the carboxy-terminus of B-type lamins is responsible for the growth of the nuclear membrane (34, 35). This may result from the insertion of this hydrophobic moiety into the membrane lipid bilayer or by interaction with a putative receptor (33). The terminal cysteine modifications are abnormally conserved in progerin (20) and may allow this truncated prelamin A to preferentially associate with lamin B1 and induce abnormal membrane biogenesis via the same mechanisms. In support with our model, similar altered nuclear phenotypes occur in mouse cells that accumulate full-length prelamin A

due to a deficiency in the expression of the Zmpste24 endoprotease (6, 9), a reversal of the phenotype being achieved by blocking farnesyltransferase (19-23).

The assembly of progerin with B-type and A-type lamins in an abnormal network may also modify the interactions of these lamins with their respective partners in adjacent structures (16, 33, 36). Ultrastructural modifications of the lamina and peripheral heterochromatin are observed in nuclei of subjects with HGPS, together with an alteration in the distribution of nuclear pore complexes in the nuclear envelope (24). Ultrastructural chromatin abnormalities are also present in nuclei from Zmpste24-deficient mice (37). Finally, the loss of A-type and B-type polymer segregation may also disturb the interactions of the lamina with various partners, generating pleiotropic downstream cellular events such as upregulation of p53 target genes (38), defective DNA repair (37), and impairment of DNA replication and transcriptional activity (24), finally leading to increased apoptosis and abnormal proliferation (39).

The tdFLIM technique is an appropriate method to analyze the changes of lamina structure in living cells expressing either progerin or various mutated lamins A responsible for numerous severe disorders (16). It also represents a promising quantitative approach to evaluate reversal to a normal phenotype in the development of therapeutic strategies.

MATERIALS AND METHODS

Plasmid constructions

pEGFP-lamin B1 and POM121-EGFP$_3$ were gifts of Dr. J. Ellenberg (EMBL, Heidelberg). The pEGFP-prelamin A construct has been described (40). The pDsRed-lamin A and pDsRed-lamin B1 constructs were produced in pDsRed-C1 vectors (Clontech Laboratories, Inc.) with DsRed in frame at the amino terminus of the full-length cDNAs of lamins. Intra-EGFP-prelamin A constructed was made following a three-step cloning strategy. From the pEGFP-prelamin A plasmid, a cDNA encoding the first 414 residues of prelamin A (prelamin A (1-414)) was amplified by PCR, with an *Eco*RI restriction site engineered at the 5' end of the sense primer (5'-GCG AAT TCT ATG GAG ACC CCG TCC CAG GGG-3') and a *Kpn*I site engineered at the 5' end of the antisense primer (5'-GC GGT ACC CCC ACC CTG TGT CTG GGA TGA-3') (restriction sites underlined). The reaction products were digested with *Eco*RI and *Kpn*I and ligated into the *Eco*RI and *Kpn*I sites of pSVK3 (Amersham Pharmacia Biotech, Inc.) similarly digested. From the pEGFP-C1 plasmid, the EGFP cDNA was amplified by PCR, with a *Kpn*I site engineered at the 5' end of the sense primer (5'-GC GGT ACC ATG GTG AGC AAG GGC GAG GAG-3') and a *Bam*H1 site engineered at the 5' end of the antisense primer (5'-GC GGA TCC CTT GTA CAG CTC GTC CAT GCC-3'). The reaction products were digested with *Bam*H1 and *Kpn*I and ligated into the *Bam*H1 and *Kpn*I sites of pSVK3-prelamin A (1-414) similarly digested. From pEGFP-prelamin A, a cDNA encoding the last 220 residues of prelamin A was amplified by PCR, with a *Bam*H1 site engineered at the 5' end of the sense primer (5'-GC GGA TCC AGC GTC ACC AAA AAG CGC AAA-3') and an *Xho*1 site engineered at the 5' end of the antisense primer (5'-GC CTC GAG TTA CAT GAT GCT GCA GTT CTG-3'). The reaction products were digested with *Bam*H1 and *Xho*1 and ligated into the *Bam*H1 and *Xho*1 sites of pSVK3-prelamin A (1-414)-EGFP similarly digested.

From pEGFP-prelamin A and pDsRed-prelamin A, the sequence corresponding to a region in the carboxy-terminal domain of prelamin A was removed by digestion with *San*DI and *Acc65*I and replaced by the DNA sequence specific of progerin (internal deletion of base pairs (bp) 1819 to 1968; residues 607 to 656). The dsDNA sequence corresponding to the carboxy-terminal fragment of progerin was obtained from oligonucleotides synthesized by Proligo Primers

and Probes (Proligo France). The first couple of single strand (ss) oligonucleotides was designed to correspond to the *LMNA* gene from bp 1723 to 1772 with a *San*DI site in the 5' end of the sense oligonucleotide (sense oligonucleotide : 5'-<u>GAC CCC</u> GCT GAG TAC AAC CTG CGC TCG CGC ACC GTG CTG TGC GGG ACC TG-3'; antisense oligonucleotide 5'-TG CCC GCA GGT CCC GCA CAG CAC GGT GCG CGA GCG CAG GTT GTA CTC AGC GGG-3'). The second couple of ss oligonucleotides was designed to correspond to bp 1773-1818 of the LMNA gene followed by bp 1969-1992, extended with *CTTA* and an *Acc*651 site at the 5' end of the antisense oligonucleotide (sense oligonucleotide 5'-C GGG CAG CCT GCC GAC AAG GCA TCT GCC AGC GGC TCA GGA GCC CAG AGC CCC AGA ACT GCA GCA TCA TGT AA G-3'; antisense oligonucleotide 5'-<u>GT AC</u>*C TTA* CAT GAT GCT GCA GTT CTG GGG CTC TG GGC TCC TGA GCC GCT GGC AGA TGC CTT GTC GGC AGG C-3'). After duplex formation, the two double strand (ds) oligonucleotides were annealed and the purified ds DNA sequence (154 bp) was inserted either into the pEGFP-prelamin A or into pDsRed1-prelamin A vector previously digested with *San*DI and *Acc*651.

tdFLIM acquisitions

The apparatus used for FRET determination performs tdFLIM by the time- and space-correlated single photon counting method (41). This method directly gives the picosecond (ps) time-resolved fluorescence decay for every pixel by counting and sampling single emitted photons according to i) the time delay between photon arrival and laser pulse (ps time scale, 4096 channels), and ii) their xy coordinate (256x256 pixel image). A titanium sapphire laser (Millennia 5W/Tsunami 3960-M3BB-UPG kit, Spectra-Physics, France) that delivers ps pulses was tuned at 960 nm to obtain an excitation wavelength at 480 nm after frequency doubling. The repetition rate was 4 MHz after pulse-picker (Spectra-physics 3980-35, France). The laser beam was expanded and inserted into an inverted epifluorescence microscope (Leica DMIRBE, France) for wide field illumination (a few mW/cm^2). The microscope stage was equipped with an incubator system for temperature and CO_2 regulation (37°C, 5 % CO_2). Green fluorescence decay images were taken using a Leica Plan-Apochromat 100X 1.3NA oil objective, a dichroic beam splitter (505DRLP; Omega; Optophotonics, Eaubonne, France), an emission filter (535DF35; Omega; Optophotonics, Eaubonne, France), and the quadrant-anode TSCSPC detector (QA, Europhoton GmbH, Germany). The band pass emission filter (515 nm < λ_{em} < 560 nm) was chosen to select

the donor fluorescence (EGFP) and to reject the acceptor fluorescence (DsRed). The count rate was up to 50 kHz. Acquisition of fluorescence decay images was done after accumulation of sufficient single photon events, usually 3 to 6 min. A temporal resolution of less than 100 ps and a spatial resolution of 500 nm were determined previously for this system (41).

tdFLIM data analysis using a three exponential model

For qualitative determination of FRET, the fluorescence decays of EGFP within the regions of interest were extracted from the acquisition matrix and the decays of EGFP-tagged lamins (donor) in the presence of DsRed-tagged lamins (acceptor) were compared with the control decays of the EGFP-tagged proteins measured in the absence of acceptor. To perform the quantitative analysis of FRET, the experimental fluorescence decays were further deconvoluted with the instrument response function and fitted by a Marquardt nonlinear least-square algorithm using Globals Unlimited software (University of Illinois at Urbana, Champain) with discrete lifetimes as theoretical model.

For each tdFLIM experiment, the fluorescence decays of EGFP in cells expressing EGFP-tagged proteins alone (monotransfected cells) or with DsRed-tagged proteins (cotransfected cells) were analyzed. The fluorescence decay of EGFP-tagged proteins in monotransfected cells was monoexponential with a lifetime of 2.27 ns ± 0.07 ns in C2C12 cells (n = 136). As the DsRed protein emits a weak green fluorescence before maturation *in vitro* (42) as well as *in vivo* (43), the decays of the green species of DsRed (Supplementary Material, Figure S1) in the 515 and 560 nm interval were analyzed and found to fit with a 2-exponential model, with lifetimes of 2.30 ± 0.50 ns and 0.24 ±0.07 ns in C2C12 cells (n = 51), and 2.54 ± 0.26 ns and 0.25 ± 0.02 ns in P19 cells (n = 17), respectively. These values were consistent with those previously found *in vitro* and *in vivo* (44, 45). The component with the shorter lifetime was 89 to 96%. In cotransfected cells in which the fluorescence decay was more rapid than in monotransfected cells, FRET analyses were carried out by fitting the fluorescence decays of EGFP using a 3-exponential model. For C2C12 and P19 cells, the fluorescence lifetime of free EGFP-lamins (τ_{EGFP}) was fixed at 2.27 ns and 2.26 ns, and that of the major component of the green species of DsRed-lamins (τ_{DsRed}) at 0.24 ns and 0.25 ns, respectively. The third lifetime corresponding to FRET (τ_{FRET}) remained free. In

cotransfected cells, the time-dependent fluorescence decay I(t) in the selected area is given by the sum:

$$I(t) = \alpha_{EGFP}.e^{-t/\tau EGFP} + \alpha_{DsRed}.e^{-t/\tau DsRed} + \alpha_{FRET}.e^{-t/\tau FRET}$$

in which α_{EGFP}, α_{DsRed} and α_{FRET} are the corresponding pre-exponential factors.

Calculation of FRET features

The proportion of EGFP-tagged proteins involved in FRET corresponds to the ratio

$$\alpha_{FRET} / (\alpha_{EGFP} + \alpha_{FRET})$$

The value of this ratio varied as a function of the intensity of the acceptor (DsRed) fluorescence, similarly for all couples of lamins analyzed in the present study (see Supplementary Material, Figure S2).

The real FRET efficiency (E) can be calculated by the equation

$$E = 1 - \tau_{FRET}/\tau_{EGFP}$$

E depends on the distance separating the donor and acceptor fluorophores and on their orientations. In most of the experiments presented here, lamins are tagged at their amino-terminal end (Fig. 1A). Once lamins tagged at this site are incorporated in the lamina, the orientation of their fluorophores is expected to be the same. We therefore interprete the differences in E values found for various lamin combinations as mostly reflecting differences in the distances separating the tagged lamins in the lamina. To a lower τ_{FRET} corresponds a higher transfer efficiency, indicative of a shorter distance (R) between the chromophores engaged in FRET, following the equation:

$$E = R_0^6 / (R_0^6 + R^6)$$

where the Förster distance R_0 corresponds to the distance at which 50 % efficiency of energy transfer takes place. In the case of fluorophores that move freely, R_0 is 4.7 nm for the couple EGFP and DsRed (46).

The percentage of cells with detectable FRET varies as a function of the acceptor to donor expression ratio. The relative quantity of EGFP- and DsRed-tagged proteins in transfected cells was calculated from additional green and red fluorescence intensity images acquired using appropriate filter cubes, a mercury lamp and a conventional CCD camera (Silar, St Petersburg, Russia). The intensities of EGFP (I_{GFP}) and DsRed (I_{Red}) signals were estimated in arbitrary units separately for green and red images. The mean gray level of regions of the nuclear envelope was calculated by taking into account the exposure time and excitation level, allowing for a comparison of the signals between different cells. FRET was measured in cells in which the acceptor was in excess over the donor, with a ratio I_{Red}/I_{GFP} (R/G) between 2 and 25. I_{GFP} was above 2 (maximum 50) and I_{Red} above 10 (maximum 300). Global analysis of the data shows that the 15 value for the R/G ratio divides the data into two classes. Above this value, nearly 100% of cells generate FRET signals whatever the lamin combination (Table 2). Below this saturation value, the percentage of cells generating FRET signals was highly dependent upon the lamin combination (Table 2). Therefore, the latter condition was used to determine if some lamin conditions were more favorable than others to trigger FRET.

Cell culture and transfections

The original mouse myoblast C2C12 cell line was grown in DMEM medium containing 15 % fetal calf serum (FCS), 1 mM glutamine, and 1 % antibiotics (100 units/ml penicillin and 100 µg/ml streptomycin). Mitotic C2C12 cells accumulated by overnight culture in the presence of 40 ng/ml nocodazole. Mouse embryonic P19 cells were grown in α-MEM medium containing 7.5 % FCS and identical additives. Cells grown to 50 % confluency in chamber slides were transfected using FuGene6 (Roche Diagnostic Co., Indianapolis, USA) following the manufacturer's instructions. Cells were used 40 to 48 hours after transfection.

Immunoblotting and fluorescence microscopy

Both methods were performed as previously described (31, 32, 40).

Statistical analysis

In Table 1, real FRET efficiencies were compared using the Student T-test. Percentages of cells positive for FRET (Table 2) were compared using the Chi-square test.

ACKNOWLEDGEMENTS

REFERENCES

1. Stuurman, N., Heins, S. and Aebi, U. (1998) Nuclear lamins: their structure, assembly, and interactions. *J. Struct. Biol.,* **122,** 42-66.
2. Daigle, N., Beaudouin, J., Hartnell, L., Imreh, G., Hallberg, E., Lippincott-Schwartz, J. and Ellenberg, J. (2001) Nuclear pore complexes form immobile networks and have a very low turnover in live mammalian cells. *J. Cell Biol.,* **154,** 71-84.
3. Hutchison, C.J. (2002) Lamins: building blocks or regulators of gene expression? *Nat. Rev. Mol. Cell Biol.,* **3,** 848-858.
4. Lin, F. and Worman, H.J. (1993) Structural organization of the human gene encoding nuclear lamin A and nuclear lamin C. *J. Biol. Chem.,* **268,** 16321-16326.
5. Rober, R.A., Weber, K. and Osborn, M. (1989) Differential timing of nuclear lamin A/C expression in the various organs of the mouse embryo and the young animal: a developmental study. *Development,* **105,** 365-378.
6. Pendas, A.M., Zhou, Z., Cadinanos, J., Freije, J.M., Wang, J., Hultenby, K., Astudillo, A., Wernerson, A., Rodriguez, F., Tryggvason, K. *et al.* (2002) Defective prelamin A processing and muscular and adipocyte alterations in Zmpste24 metalloproteinase-deficient mice. *Nat. Genet.,* **31,** 94-99.
7. Sinensky, M. (2000) Functional aspects of polyisoprenoid protein substituents: roles in protein-protein interaction and trafficking. *Biochim. Biophys. Acta,* **1529,** 203-209.
8. Young, S.G., Fong, L.G. and Michaelis, S. (2005) Thematic review series: Lipid posttranslational modifications. Prelamin A, Zmpste24, misshapen cell nuclei, and progeria--new evidence suggesting that protein farnesylation could be important for disease pathogenesis. *J. Lipid Res.,* **46,** 2531-2558.
9. Bergo, M.O., Gavino, B., Ross, J., Schmidt, W.K., Hong, C., Kendall, L.V., Mohr, A., Meta, M., Genant, H., Jiang, Y. *et al.* (2002) Zmpste24 deficiency in mice causes spontaneous bone fractures, muscle weakness, and a prelamin A processing defect. *Proc. Natl Acad. Sci. USA,* **99,** 13049-13054.
10. Corrigan, D.P., Kuszczak, D., Rusinol, A.E., Thewke, D.P., Hrycyna, C.A., Michaelis, S. and Sinensky, M.S. (2005) Prelamin A endoproteolytic processing in vitro by recombinant Zmpste24. *Biochem. J.,* **387,** 129-138.
11. Gieffers, C. and Krohne, G. (1991) In vitro reconstitution of recombinant lamin A and a lamin A mutant lacking the carboxy-terminal tail. *Eur. J. Cell Biol.,* **55,** 191-199.
12. Moir, R.D., Donaldson, A.D. and Stewart, M. (1991) Expression in Escherichia coli of human lamins A and C: influence of head and tail domains on assembly properties and paracrystal formation. *J. Cell Sci.,* **99 (Pt 2),** 363-372.
13. Heitlinger, E., Peter, M., Lustig, A., Villiger, W., Nigg, E.A. and Aebi, U. (1992) The role of the head and tail domain in lamin structure and assembly: analysis of bacterially expressed chicken lamin A and truncated B2 lamins. *J. Struct. Biol.,* **108,** 74-89.
14. Schirmer, E.C. and Gerace, L. (2004) The stability of the nuclear lamina polymer changes with the composition of lamin subtypes according to their individual binding strengths. *J. Biol. Chem.,* **279,** 42811-42817.
15. Ye, Q. and Worman, H.J. (1995) Protein-protein interactions between human nuclear lamins expressed in yeast. *Exp. Cell Res.,* **219,** 292-298.
16. Worman, H.J. and Courvalin, J.C. (2005) Nuclear envelope, nuclear lamina, and inherited disease. *Int. Rev. Cytol.,* **246,** 231-279.
17. Eriksson, M., Brown, W.T., Gordon, L.B., Glynn, M.W., Singer, J., Scott, L., Erdos, M.R., Robbins, C.M., Moses, T.Y., Berglund, P. *et al.* (2003) Recurrent de novo point mutations in lamin A cause Hutchinson-Gilford progeria syndrome. *Nature,* **423,** 293-298.
18. De Sandre-Giovannoli, A., Bernard, R., Cau, P., Navarro, C., Amiel, J., Boccaccio, I., Lyonnet, S., Stewart, C.L., Munnich, A., Le Merrer, M. *et al.* (2003) Lamin A truncation in Hutchinson-Gilford progeria. *Science,* **300,** 2055.
19. Toth, J.I., Yang, S.H., Qiao, X., Beigneux, A.P., Gelb, M.H., Moulson, C.L., Miner, J.H., Young, S.G. and Fong, L.G. (2005) Blocking protein farnesyltransferase improves nuclear shape in fibroblasts from humans with progeroid syndromes. *Proc. Natl Acad. Sci. USA,* **102,** 12873-12878.

20. Glynn, M.W. and Glover, T.W. (2005) Incomplete processing of mutant lamin A in Hutchinson-Gilford progeria leads to nuclear abnormalities, which are reversed by farnesyltransferase inhibition. *Hum. Mol. Genet.,* **14,** 2959-2969.

21. Capell, B.C., Erdos, M.R., Madigan, J.P., Fiordalisi, J.J., Varga, R., Conneely, K.N., Gordon, L.B., Der, C.J., Cox, A.D. and Collins, F.S. (2005) Inhibiting farnesylation of progerin prevents the characteristic nuclear blebbing of Hutchinson-Gilford progeria syndrome. *Proc. Natl Acad. Sci. USA,* **102,** 12879-12884.

22. Mallampalli, M.P., Huyer, G., Bendale, P., Gelb, M.H. and Michaelis, S. (2005) Inhibiting farnesylation reverses the nuclear morphology defect in a HeLa cell model for Hutchinson-Gilford progeria syndrome. *Proc. Natl Acad. Sci. USA,* **102,** 14416-14421.

23. Yang, S.H., Bergo, M.O., Toth, J.I., Qiao, X., Hu, Y., Sandoval, S., Meta, M., Bendale, P., Gelb, M.H., Young, S.G. *et al.* (2005) Blocking protein farnesyltransferase improves nuclear blebbing in mouse fibroblasts with a targeted Hutchinson-Gilford progeria syndrome mutation. *Proc. Natl Acad. Sci. USA,* **102,** 10291-10296.

24. Goldman, R.D., Shumaker, D.K., Erdos, M.R., Eriksson, M., Goldman, A.E., Gordon, L.B., Gruenbaum, Y., Khuon, S., Mendez, M., Varga, R. *et al.* (2004) Accumulation of mutant lamin A causes progressive changes in nuclear architecture in Hutchinson-Gilford progeria syndrome. *Proc. Natl Acad. Sci. USA,* **101,** 8963-8968.

25. Scaffidi, P. and Misteli, T. (2005) Reversal of the cellular phenotype in the premature aging disease Hutchinson-Gilford progeria syndrome. *Nat. Med.,* **11,** 440-445.

26. Stewart, C. and Burke, B. (1987) Teratocarcinoma stem cells and early mouse embryos contain only a single major lamin polypeptide closely resembling lamin B. *Cell,* **51,** 383-392.

27. Soderqvist, H. and Hallberg, E. (1994) The large C-terminal region of the integral pore membrane protein, POM121, is facing the nuclear pore complex. *Eur. J. Cell Biol.,* **64,** 186-191.

28. Moir, R.D., Yoon, M., Khuon, S. and Goldman, R.D. (2000) Nuclear lamins A and B1: different pathways of assembly during nuclear envelope formation in living cells. *J. Cell Biol.,* **151,** 1155-1168.

29. Izumi, M., Vaughan, O.A., Hutchison, C.J. and Gilbert, D.M. (2000) Head and/or CaaX domain deletions of lamin proteins disrupt preformed lamin A and C but not lamin B structure in mammalian cells. *Mol. Biol. Cell,* **11,** 4323-4337.

30. Gerace, L. and Blobel, G. (1980) The nuclear envelope lamina is reversibly depolymerized during mitosis. *Cell,* **19,** 277-287.

31. Favreau, C., Dubosclard, E., Ostlund, C., Vigouroux, C., Capeau, J., Wehnert, M., Higuet, D., Worman, H.J., Courvalin, J.C. and Buendia, B. (2003) Expression of lamin A mutated in the carboxyl-terminal tail generates an aberrant nuclear phenotype similar to that observed in cells from patients with Dunnigan-type partial lipodystrophy and Emery-Dreifuss muscular dystrophy. *Exp. Cell Res.,* **282,** 14-23.

32. Vigouroux, C., Auclair, M., Dubosclard, E., Pouchelet, M., Capeau, J., Courvalin, J.C. and Buendia, B. (2001) Nuclear envelope disorganization in fibroblasts from lipodystrophic patients with heterozygous R482Q/W mutations in the lamin A/C gene. *J. Cell Sci.,* **114,** 4459-4468.

33. Maske, C.P., Hollinshead, M.S., Higbee, N.C., Bergo, M.O., Young, S.G. and Vaux, D.J. (2003) A carboxyl-terminal interaction of lamin B1 is dependent on the CAAX endoprotease Rce1 and carboxymethylation. *J. Cell Biol.,* **162,** 1223-1232.

34. Prufert, K., Vogel, A. and Krohne, G. (2004) The lamin CxxM motif promotes nuclear membrane growth. *J. Cell Sci.,* **117,** 6105-6116.

35. Ralle, T., Grund, C., Franke, W.W. and Stick, R. (2004) Intranuclear membrane structure formations by CaaX-containing nuclear proteins. *J. Cell Sci.,* **117,** 6095-6104.

36. Barton, R.M. and Worman, H.J. (1999) Prenylated prelamin A interacts with Narf, a novel nuclear protein. *J. Biol. Chem.,* **274,** 30008-30018.

37. Liu, B., Wang, J., Chan, K.M., Tjia, W.M., Deng, W., Guan, X., Huang, J.D., Li, K.M., Chau, P.Y., Chen, D.J. *et al.* (2005) Genomic instability in laminopathy-based premature aging. *Nat. Med.,* **11,** 780-785.

38. Varela, I., Cadinanos, J., Pendas, A.M., Gutierrez-Fernandez, A., Folgueras, A.R., Sanchez, L.M., Zhou, Z., Rodriguez, F.J., Stewart, C.L., Vega, J.A. *et al.* (2005) Accelerated ageing in mice deficient in Zmpste24 protease is linked to p53 signalling activation. *Nature,* **437,** 564-568.

39. Bridger, J.M. and Kill, I.R. (2004) Aging of Hutchinson-Gilford progeria syndrome fibroblasts is characterised by hyperproliferation and increased apoptosis. *Exp. Gerontol.,* **39,** 717-724.

40. Favreau, C., Higuet, D., Courvalin, J.C. and Buendia, B. (2004) Expression of a mutant lamin A that causes Emery-Dreifuss muscular dystrophy inhibits in vitro differentiation of C2C12 myoblasts. *Mol. Cell. Biol.,* **24,** 1481-1492.

41. Emiliani, V., Sanvitto, D., Tramier, M., Piolot, T., Petrasek, Z., Kemnitz, K., Durieux, C. and Coppey-Moisan, M. (2003) Low-intensity two-dimensional imaging of fluorescence lifetimes in living cells. *Appl. Phys. Lett.,* **83,** 2471-2473.

42. Baird, G.S., Zacharias, D.A. and Tsien, R.Y. (2000) Biochemistry, mutagenesis, and oligomerization of DsRed, a red fluorescent protein from coral. *Proc. Natl Acad. Sci. USA,* **97,** 11984-11989.

43. Terskikh, A.V., Fradkov, A.F., Zaraisky, A.G., Kajava, A.V. and Angres, B. (2002) Analysis of DsRed mutants. Space around the fluorophore accelerates fluorescence development. *J. Biol. Chem.,* **277,** 7633-7636.

44. Cotlet, M., Hofkens, J., Habuchi, S., Dirix, G., Van Guyse, M., Michiels, J., Vanderleyden, J. and De Schryver, F.C. (2001) Identification of different emitting species in the red fluorescent protein DsRed by means of ensemble and single-molecule spectroscopy. *Proc. Natl Acad. Sci. USA,* **98,** 14398-14403.

45. Tramier, M., Gautier, I., Piolot, T., Ravalet, S., Kemnitz, K., Coppey, J., Durieux, C., Mignotte, V. and Coppey-Moisan, M. (2002) Picosecond-hetero-FRET microscopy to probe protein-protein interactions in live cells. *Biophys. J.,* **83,** 3570-3577.

46. Patterson, G.H., Piston, D.W. and Barisas, B.G. (2000) Forster distances between green fluorescent protein pairs. *Anal. Biochem.,* **284,** 438-440.

LEGENDS TO FIGURES

Figure 1. Overexpressed tagged lamins, wild-type or mutated (progerin) are integrated within the lamina. (A) Schematic diagram of the lamins expressed by the plasmid constructs. Numbers refer to the amino acids of lamin proteins. The large box represents the dimerization rod domain. The small squares and triangles correspond to the EGFP and DsRed fluorophores, respectively. La A, La B1 and Pgn refer to lamin A, lamin B1 and progerin, respectively. (B) Endogenous and exogenous lamins are similarly resistant to extraction. Control C2C12 cells (upper panels) and C2C12 cells coexpressing tagged lamin A (DsRed-La A) and lamin B1 (EGFP-La B1) (middle panels), or expressing tagged progerin (EGFP-Pgn) (lower panels), were sequentially extracted with Triton X-100 (TX), Triton and salt (TX-NaCl), and finally digested with DNase I and RNase A followed by salt extraction (TX-N-DNase). The three supernatants (TX, TX-NaCl, TX-N-DNase) and the final insoluble fraction (Ins) were analyzed by immunoblotting. In left panels, endogenous lamins A and C (La A and La C) and DsRed-lamin A (DsRed-La A) were revealed by rabbit antibodies directed against lamins A and C, and EGFP-progerin (EGFP-Pgn) was revealed by a monoclonal antibody directed against GFP. In right panels, endogenous lamin B1 (La B1) and exogenous lamin B1 (EGFP-La B1) were revealed by rabbit antibodies directed against lamin B1. Each lane corresponds to material extracted from $5x10^4$ cells. The amount of extracted proteins in each fraction (supernatants and pellet), as judged by Ponceau red staining (not shown), was similar in all experiments.

Figure 2. Overexpressed tagged lamins localize at the nuclear envelope in C2C12 (A) and P19 (B) cells. Endogenous lamins A and C (La A/C) and B1 (La B1) are revealed by indirect immunofluorescence in C2C12 and in P19 cells, using antibodies against lamins A and C (anti-LaA/C) and antibodies against lamin B1 (anti-La B1). Note that A-type lamins are not expressed in P19 cells. Exogenous EGFP- or DsRed- tagged wild-type lamins and progerin (Pgn), detected by direct fluorescence, localize at the nuclear periphery. The nuclei in some C2C12 cells expressing progerin are larger than usual and dysmorphic (arrows) with extensive nuclear envelope folding (arrowheads). A similar folding is also observed in some cells expressing exogenous lamin B1 (arrowheads). Bars = 10 µm.

23

Figure 3. Heterotypic and homotypic interactions between tagged lamins are detected by FRET. C2C12 cells were mono- and cotransfected as indicated. Steady-state fluorescence images were acquired with a CCD camera (CCD panels). Time integrated images obtained for each cell with the quadrant anode detector are presented in the Quadrant panels. Nuclear envelope domains (highlighted in yellow in Quadrant panels) were selected, and corresponding fluorescent decays are normalized and plotted in the graphs. Green and blue curves refer to fluorescence decays in mono- and cotransfected cells, respectively. (A) FRET occurs in cells coexpressing tagged lamins A (La A) and B1 (La B1). (B) FRET is not detected in cells coexpressing tagged lamin B1 and Pom121. (C) FRET occurs in cells coexpressing EGFP- and DsRed-tagged lamin B1. ns refers to nanosecond. Bars = 10 µm.

Figure 4. Hypothetical models of lamina structure represented in a transverse section of the nuclear envelope. (A) Schematic cross-sectional representation of possible polymer assembly of A- and B-type lamins in the lamina. In model 1, lamins are integrated into homopolymers that are not in contact. In model 2, both types of lamins are integrated into mixed polymers where they are evenly distributed. In model 3, lamins of both types interact but they are not evenly distributed. They are integrated either in a heteropolymeric structure or in two homopolymers that are in contact. (B) In a somatic cell, wild-type A- and B-type lamins form homopolymers that interact. Due to the insertion of the farnesyl group (squiggly line) into the inner nuclear membrane, B-type polymers are more closely associated with the membrane than A-type polymers. Since lamina is a fenestrated structure, a fraction of the chromatin is represented in contact with the membrane. (C) In a cell expressing progerin, farnesylated progerin assembles with B-type lamins to form mix heteropolymers, while homopolymerization of B-type lamins is abolished. Since progerin still associates with a fraction of wild-type lamin A, the new mixed polymer of lamin B and progerin, also contains lamin A (B-P-A).

TABLES

Table 1. FRET lifetimes and real FRET efficiencies in cells expressing EGFP and DsRed tagged lamins.

Coexpressed tagged proteins	FRET lifetime τ_{FRET} (ns)	Real FRET efficiency $E = 1 - \tau_{FRET}/\tau_{EGFP}$	Cell number
Interphasic C2C12 cells : $\tau_{EGFP} = 2.27 \pm 0.07$ ns			*136*
DsRed-La B1 / EGFP-La A	0.76 ± 0.09	0.66 ± 0.04*	10
DsRed-La A / EGFP-La B1	0.80 ± 0.09	0.65 ± 0.04*	22
DsRed-La A / EGFP-La A	0.83 ± 0.09	0.64 ± 0.04*	21
DsRed-La B1 / EGFP-La B1	1.00 ± 0.08	0.57 ± 0.04	23
DsRed-Pgn / EGFP-Pgn	0.96 ± 0.17	0.58 ± 0.07**	22
DsRed-Pgn / EGFP-La B1	1.01 ± 0.16	0.56 ± 0.07**	27
DsRed-Pgn / EGFP-La A	0.93 ± 0.10	0.59 ± 0.05**	15
Interphasic P19-EC cells : $\tau_{EGFP} = 2.26 \pm 0.02$ ns			*27*
DsRed-La B1 / EGFP-La B1	0.78 ± 0.12	0.65 ± 0.05***	30
DsRed-La A/ EGFP-La B1	0.80 ± 0.13	0.65 ± 0.05	12

FRET lifetimes (τ_{FRET}) and real FRET efficiencies (E) in transfected C2C12 and P19 cells. Mean τ_{FRET} values are expressed in nanoseconds (ns). In each series of experiments, τ_{EGFP} is the mean of the lifetimes of EGFP in monotransfected cells. For C2C12 and P19 cells, a total of 136 and 27 nuclei in monotransfected cells were analyzed, as indicated. For each cotransfection, monotransfection with the corresponding EGFP-tagged protein was performed. Mean τ_{FRET} and E values include standard errors.

*   P < 0.0001 *vs* DsRed-La B1 / EGFP-La B1 in C2C12 cells

**   P < 0.002 *vs* DsRed-La A / EGFP-La A
    P < 0.0004 *vs* DsRed-La A / EGFP-La B1 in C2C12 cells

***   P < 0.0001 *vs* DsRed-La B1 / DsRed-La B1 in C2C12 cells.

Table 2. Percentage of cells with detectable FRET as a function of the acceptor (Ds<u>R</u>ed) to donor (E<u>G</u>FP) expression ratio (R/G).

Coexpressed tagged proteins	R/G < 15 (%)	R/G >15 (%)
DsRed-La A / EGFP-La B1	20	92
DsRed-La A / EGFP-La A	83	100
DsRed-La B1 / EGFP-La B1	93	100
DsRed-Pgn / EGFP-Pgn	100	nd
DsRed-Pgn / EGFP-La B1	62*	100
DsRed-Pgn / EGFP-La A	nd	100
DsRed-La A / EGFP-Pgn	69	100

Abbreviations are as in Table 1. The relative quantity of DsRed- and EGFP-tagged proteins in transfected cells were calculated from fluorescence intensity measurements as described in *Materials and Methods*. Data were obtained from about 20 cells in each case and expressed as a percentage (%) of cells in which FRET was detectable. nd, not determined. Statistical data concerning this Table are presented in the text.

* P < 0,05 *vs* DsRed-La A / EGFP-La B1

ABBREVIATIONS

FRET, fluorescence resonance energy transfer; FLIM, fluorescence lifetime imaging microscopy; tdFLIM, time domain FLIM; HGPS, Hutchinson-Gilford progeria syndrome; CAAX, cysteine, aliphatic, aliphatic, one of several amino acids; EGFP, enhanced green fluorescent protein; DsRed, red fluorescent protein; n, number of nuclei.
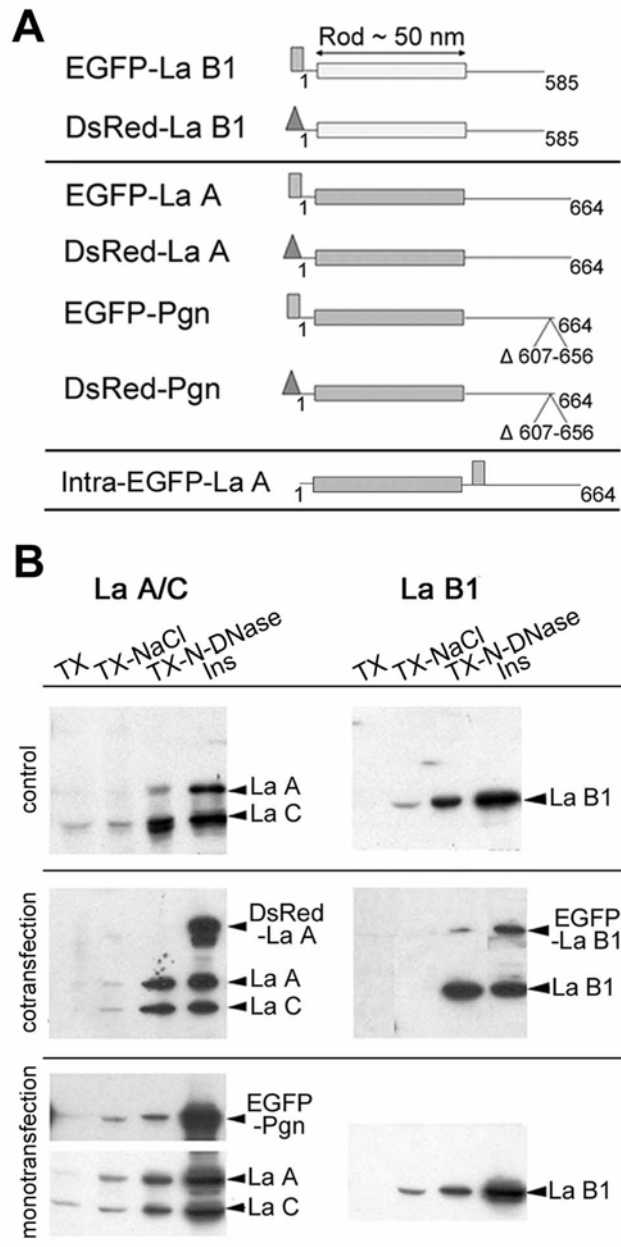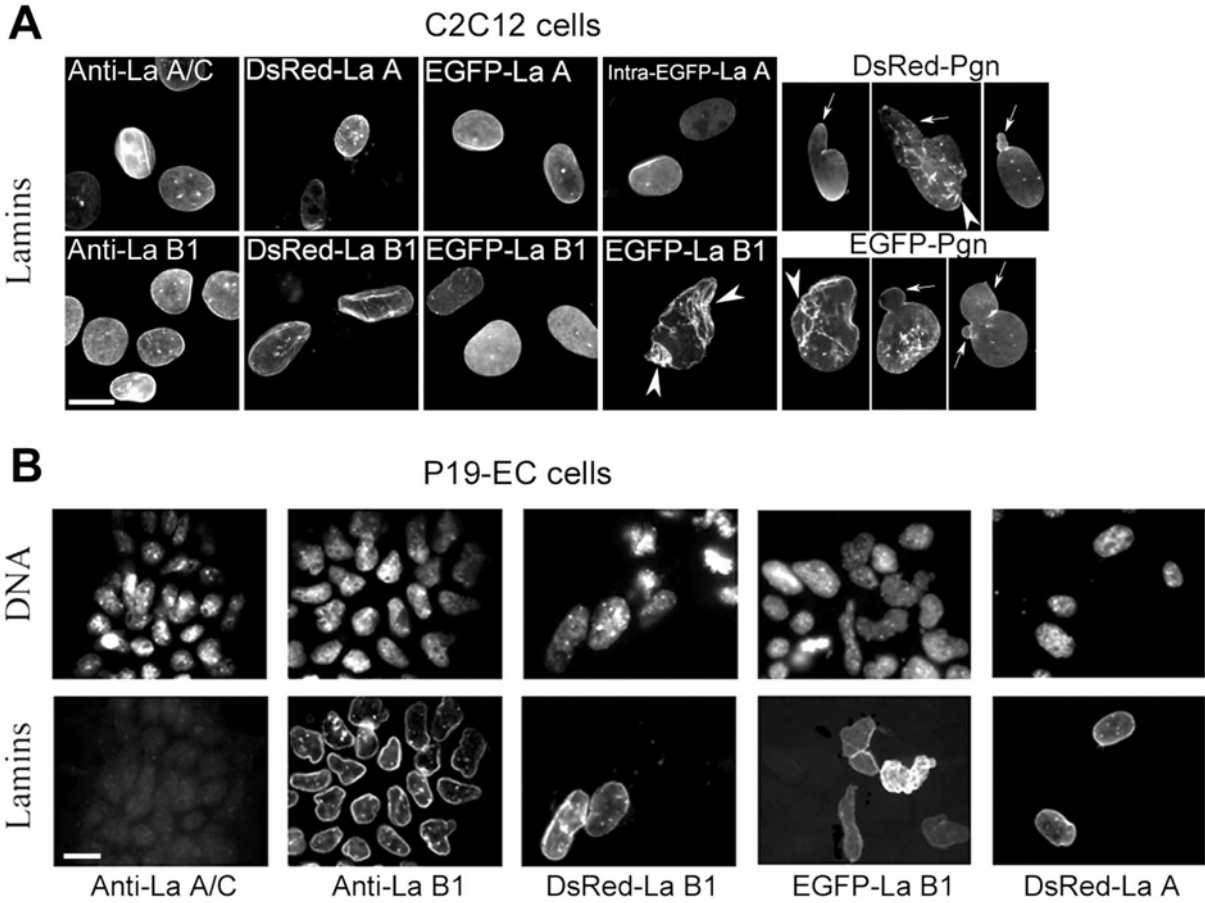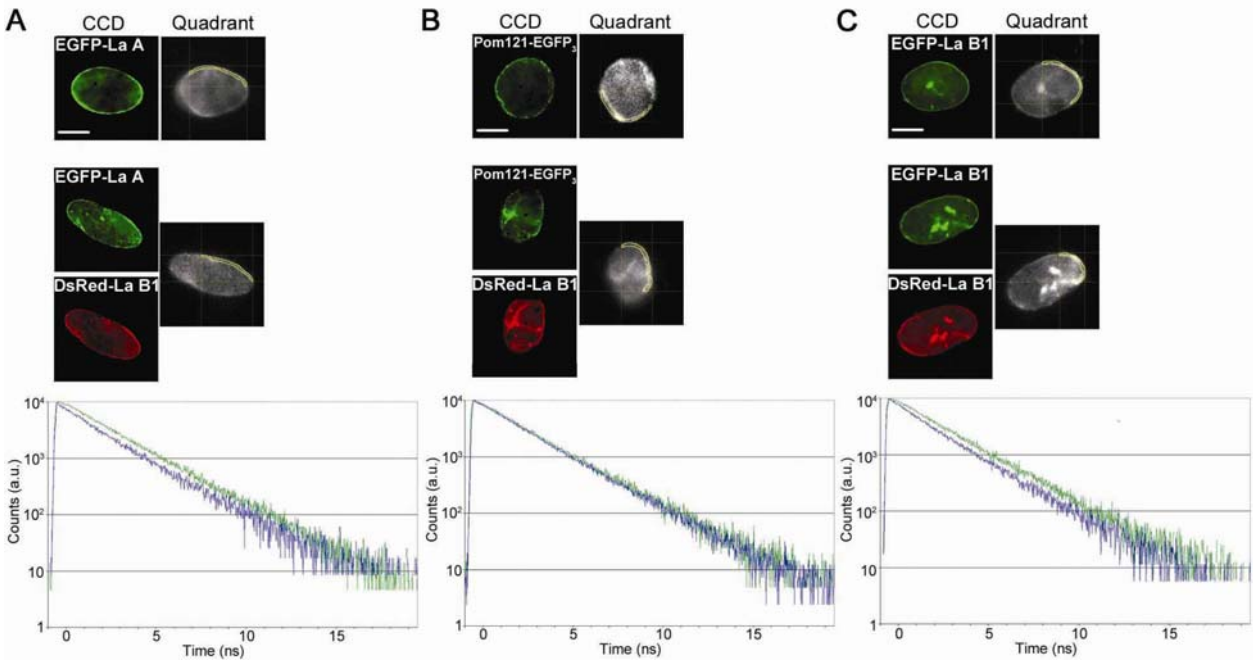
Figures

Figure 1 :

Figure 2 :

A — C2C12 cells

Lamins

| Anti-La A/C | DsRed-La A | EGFP-La A | Intra-EGFP-La A | DsRed-Pgn |
| Anti-La B1 | DsRed-La B1 | EGFP-La B1 | EGFP-La B1 | EGFP-Pgn |

B — P19-EC cells

DNA

Lamins

Anti-La A/C Anti-La B1 DsRed-La B1 EGFP-La B1 DsRed-La A

Figure 3 :

Figure 4 :